Actin and agonist MHC–peptide complex–dependent T cell receptor microclusters as scaffolds for signaling

Gabriele Campi, Rajat Varma, and Michael L. Dustin

Department of Pathology and the Program in Molecular Pathogenesis, Skirball Institute of Biomolecular Medicine, New York, NY 10016

T cell receptor (TCR) microclusters form within seconds of T cell contact with supported planar bilayers containing intercellular adhesion molecule-1 and agonist major histocompatibility complex (MHC)–peptide complexes, and elevation of cytoplasmic Ca^{2+} is observed within seconds of the first detectable microclusters. At 0–30 s after contact, TCR microclusters are colocalized with activated forms of Lck, ZAP-70, and the linker for activation of T cells. By 2 min, activated kinases are reduced in the older central microclusters, but are abundant in younger peripheral microclusters. By 5 min, TCR in the central supramolecular activation cluster have reduced activated kinases, whereas faint peripheral TCR microclusters efficiently generated activated Lck and ZAP-70. TCR microcluster formation is resistant to inhibition by Src family kinase inhibitor PP2, but is abrogated by actin polymerization inhibitor latrunculin A. We propose that Src kinase–independent formation of TCR microclusters in response to agonist MHC–peptide provides an actin-dependent scaffold for signal amplification.

CORRESPONDENCE
Michael L. Dustin:
dustin@saturn.med.nyu.edu

T cell activation is dependent upon the interaction of T cell receptors with MHC–peptide complexes in the interface between T cells and APCs (1). Molecular rearrangements after antigen recognition lead to the formation of an organized immunologic synapse (IS) that is characterized by a central cluster of T cell receptors (central supramolecular activation cluster [cSMAC]), which is surrounded by a ring of adhesion molecules (peripheral SMAC [pSMAC]) (2–4). Signaling is initiated before the formation of the IS and can proceed in the absence of IS formation (5–9). Furthermore, the large central cluster of TCRs in the cSMAC is a site where signals are down-regulated; this suggests that T cell receptor clustering may correspond to down-regulation, rather than initiation phases of TCR signaling (6, 8). Before IS formation, TCR microclusters form in the interface using cell–cell and cell-supported planar systems for studying the IS (10, 11). TCR microclusters also are formed in the interface between Jurkat T cells and glass substrates that are coated directly with anti-CD3, but do not translocate to form a cSMAC (12). These studies predict that TCR microclusters will initiate signaling through recruitment of tyrosine kinases and adaptor molecules (13, 14). However, the kinetics of signaling and requirements for formation of TCR microclusters in response to agonist MHC–peptide is unknown.

RESULTS AND DISCUSSION

Imaging of T cell activation with supported planar bilayers offers several advantages in spatial and temporal resolution, sampling efficiency, and control of conditions when compared with cell–cell imaging (15). We demonstrated previously that laterally mobile intercellular adhesion molecule (ICAM)-1 and I-E^k-moth cytochrome *c* peptide 88–103 in supported bilayers induce the proliferation of antigen-specific T cell blasts (5). In this system, previous tracking of TCRs, using confocal microscopy, and H57 Fab fragments prebound to the TCRβ subunit, revealed that TCR/MHCp microclusters form in the contact area between T cells and supported planar bilayers, and, as the cells spread on the substrate, accumulate at the periphery (11). The microclusters move to the center of the contact area to form the cSMAC by 5 min. This is identical to the kinetics of microcluster formation and translocation in cell–cell systems (7, 10, 16). To study the relationship of TCR microclusters to early T cell signaling, we used in vitro activated AND

JEM © The Rockefeller University Press $8.00
Vol. 202, No. 8, October 17, 2005 1031–1036 www.jem.org/cgi/doi/10.1084/jem.20051182

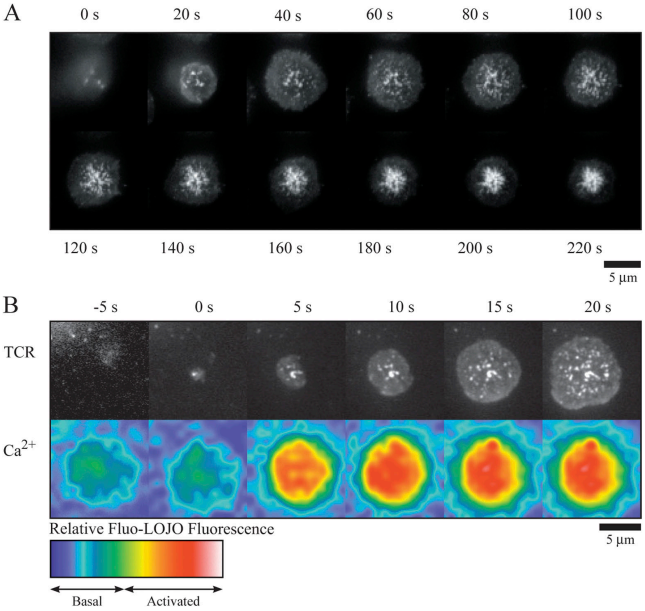

Figure 1. Dynamic of TCR microclusters during formation of a mature IS. (A) A series of images of Alexa546-H57 Fab–labeled AND TCR Tg T cell blasts interacting with planar bilayer containing ICAM-1 and agonist MHCp at times indicated. Time is relative to first detected contact area. This sequence is representative of three experiments with at least 20 cells observed in each. (B) Alexa546-H57 Fab and Fluo-LOJO dye–labeled AND TCR Tg T cell blasts interacting with planar bilayers containing ICAM-1 and agonist MHCp at early times. TIRFM of Alexa546 anti-TCR to visualize microcluster formation (top row) and wide field image of Fluo-LOJO fluorescence 4 μm above the contact plane indicates relative cytoplasmic Ca^{2+} (bottom row). The TIRFM image was acquired 1 s before the Fluo-LOJO image. Representative of three experiments.

TCR Tg T cells and supported planar bilayers containing glycosylphosphatidyl inositol anchored ICAM-1 (ICAM-1–GPI) and I-E^k-GPI with moth cytochrome *c* peptide 88–103 (agonist MHCp) at 40 molecules/μm^2. T cells formed microclusters on these bilayers with ~140 TCR each that are readily detectable by wide-field fluorescence microscopy (Fig. 1 A). We next determined the relationship of TCR microcluster formation to cytoplasmic Ca^{2+}. We used a cytoplasmic dye, Fluo-LOJO, to measure relative Ca^{2+} levels based on increased fluorescence intensity in parallel with Alexa 546-H57 Fab; through the objective, total internal reflection fluorescence microscopy (TIRFM) (17) was used to detect even small TCR microclusters. TIRFM detects fluorescence within 100–200 nm of the interface between the T cells and the planar bilayers, and thus, provides very high lateral and axial resolution at the cell–planar bilayer interface (18). Images of Fluo-LOJO fluorescence and TCR fluorescence were acquired alternately with a delay of 1 s between the TIRFM image of the TCR cluster and the image of cytoplasmic Ca^{2+}. As reported previously (19), T cells rested on the bilayer for a few seconds before initiating contact formation. During this time, the basal fluorescence of the indi-

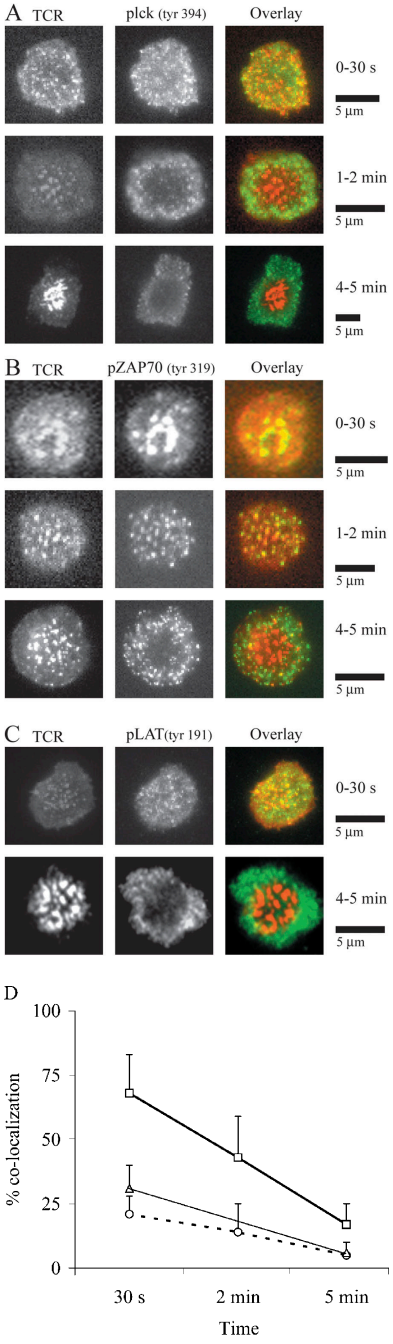

Figure 2. Relationship of pLck^{394}, pZAP-70^{319}, and pLAT^{191} to TCR microclusters during IS formation. Alexa546-H57 Fab–labeled AND TCR Tg T cells were incubated on bilayers containing ICAM-1 and MHCp. At different times after cell injection, the cells were fixed to yield contacts that formed between 0–0.5 min, 1–2 min, or 4–5 min. Cell were permeabilized and stained with antibodies to pLck^{394} (A), pZAP^{319} (B), and pLAT^{191} (C) followed by Alexa488-conjugated secondary antibodies. TCR- (red in overlay) and phosphoprotein-specific antibodies (green in overlay) were imaged by wide-field fluorescence microscopy. (D) Colocalization was quantified based on the Improvision colocalization algorithm (classifier threshold 1.5×). Microclusters from at least 10 contact areas were included for each data point.

vidual T cell was assessed. Small contacts with a single detectable TCR microcluster remained in the basal range of Fluo-LOJO fluorescence; however, contacts with two or three TCR clusters consistently displayed elevated Fluo-LOJO fluorescence (Fig. 1 B). There was a delay of ~5 s between the first detectable TCR microcluster and elevation of cytoplasmic Ca^{2+}. On bilayers with ICAM-1 only Fluo-LOJO fluorescence fluctuates in the basal region. Because of its low K_{Ca2+}, Fluo-LOJO is sensitive to basal fluctuations in cytoplasmic Ca^{2+}. Thus, T cell receptor signaling is initiated well before complete spreading of the T cell, and appearance of the first TCR microcluster precedes Ca^{2+} signaling.

We next determined the relationship of microcluster formation to activation of tyrosine kinases Lck and ζ-associated protein of 70 kD (ZAP-70) and the phosphorylation of the adaptor molecule linker of activated T cells (LAT). AND TCR Tg T cells were allowed to settle on bilayers containing ICAM-1 and agonist MHCp for 30 s, 2 min, or 5 min at 37°C; cells were fixed, permeabilized, and stained with affinity-purified antibodies to phospho-Lck tyr 394 ($pLck^{394}$) (6, 20), phospho–ZAP-70 tyr 319 ($pZAP^{319}$) (21), or phospho-LAT tyr 191 ($pLAT^{191}$) (22). The antibody to $pLck^{394}$ weakly cross reacts with autophosphorylated Fyn (20). Controls included the use of nonimmune species–matched IgG and examination of specific fluorescence on ICAM-1 only bilayers (unpublished data). At 30 s, there was a high degree of colocalization of $pLck^{394}$, $pZAP^{319}$, and $pLAT^{191}$ with TCR microclusters (Fig. 2, A–C). Early central TCR microclusters often appeared to fuse together, but were still functional (e.g., Fig. 2 A, 0–30 s). By 2 min, the TCR clusters near the center of the contact retained $pZAP^{319}$, but already showed lower levels of $pLck^{394}$, whereas more peripheral TCR microclusters still were colocalized with $pLck^{394}$ and $pZAP^{319}$. In addition to colocalizing with TCR microclusters, $pLck^{394}$ stained at a lower level in the peripheral region of the synapse just outside the pSMAC. By 5 min, the cSMAC had formed and was largely devoid of $pLck^{394}$, $pZAP^{319}$, and $pLAT^{191}$. However, the periphery still contained bright foci of all three phosphoproteins, even if TCR microclusters could not be resolved clearly. Quantification of colocalization of $pLck^{394}$, $pZAP^{319}$, and $pLAT^{191}$ with the visible TCR signal decreased over 5 min (Fig. 2 D). Therefore, these signaling events in the periphery were not mediated by the TCR, or TCR clusters were forming that were not visible by wide-field fluorescence microscopy.

We used TIRFM to determine if we could identify TCR microclusters in the periphery that would correspond to the presence of $pLck^{394}$ and $pZAP^{319}$ at 5 min. TIRFM revealed faint, but definitive, TCR clusters in the periphery at 5 min, which colocalized with the $pLck^{394}$ and $pZAP^{319}$ (Fig. 3, A and B). Thus, peripheral TCR microclusters undergo a 10-fold decrease in intensity by 5 min, but are still detected readily by TIRFM, although not by confocal or wide-field fluorescence imaging because of interference from out-of-focus fluorescence. TIRFM also increased the

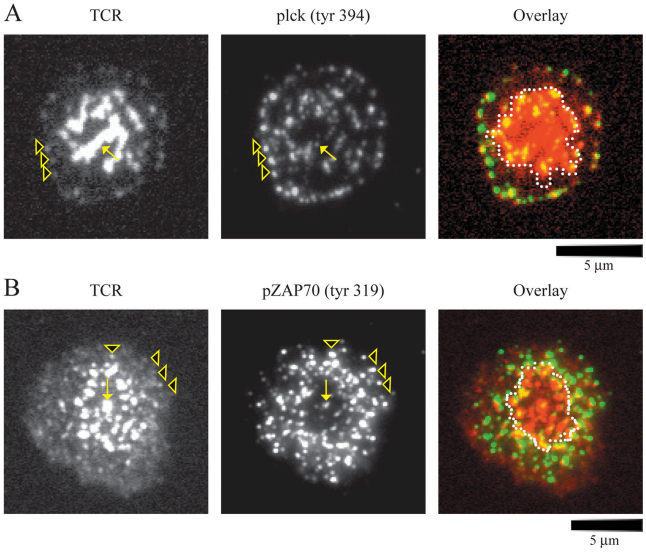

Figure 3. Colocalization of $pLck^{394}$ and $pZAP^{319}$ with peripheral TCR microclusters in the IS. Cells were prepared exactly as for 4–5-min time point in Fig. 2, and then TCR (red in overlay) and the indicated phosphoprotein (green in overlay) were imaged by TIRFM for cells stained with $pLck^{394}$ (A) and $pZAP^{319}$ (B). Examples of locations where peripheral TCR clusters colocalize with active kinases are indicated with arrowheads; positions where the large central TCR clusters contained active kinases are indicted by an arrow. The dividing line between central and peripheral structures used for calculation of the signaling efficiency is indicated in the overlay by the dotted white line. Representative of three experiments.

sensitivity of detection of $pLck^{394}$ and $pZAP^{319}$ such that signaling was detected at 5 min in the large central TCR clusters. We quantified the "signaling efficiency" as the ratio of the relevant phosphorylated kinase/TCR. At 5 min, the signaling efficiency was 30-fold higher for $pLck^{394}$ and $pZAP^{319}$ in peripheral clusters than in central clusters. Greater than 95% of $pLck^{394}$ and $pZAP^{319}$ was contained in peripheral microclusters by 5 min.

We next determined whether early TCR microclusters are formed as a consequence of signaling. PP2 is a potent inhibitor of T cell receptor signaling that inhibits all src family kinases and some additional tyrosine kinases, and blocks ZAP-70 recruitment to the activated TCR on anti-CD3 substrates (12, 23, 24). When T cells were pretreated with 20 μM PP2 and exposed to the bilayers containing ICAM-1 and agonist MHCp in the continued presence of the same concentration of PP2, AND TCR Tg T cells were able to form TCR microclusters without elevation of cytoplasmic Ca^{2+} above the basal range (Fig. 4 A). The basal fluctuations in cytoplasmic Ca^{2+} might mask signaling at the TCR, so we addressed this by directly examining the activation of Lck in the presence of PP2. The amount of $pLck^{394}$ in the contact was reduced by 91% at 20 μM PP2 and by >95% by 100 μM PP2, yet TCR microclusters still formed at both concentrations (Fig. 4 B). PP2 (10 μM) completely inhibited pSMAC formation, reduced contact size as indicated by interference

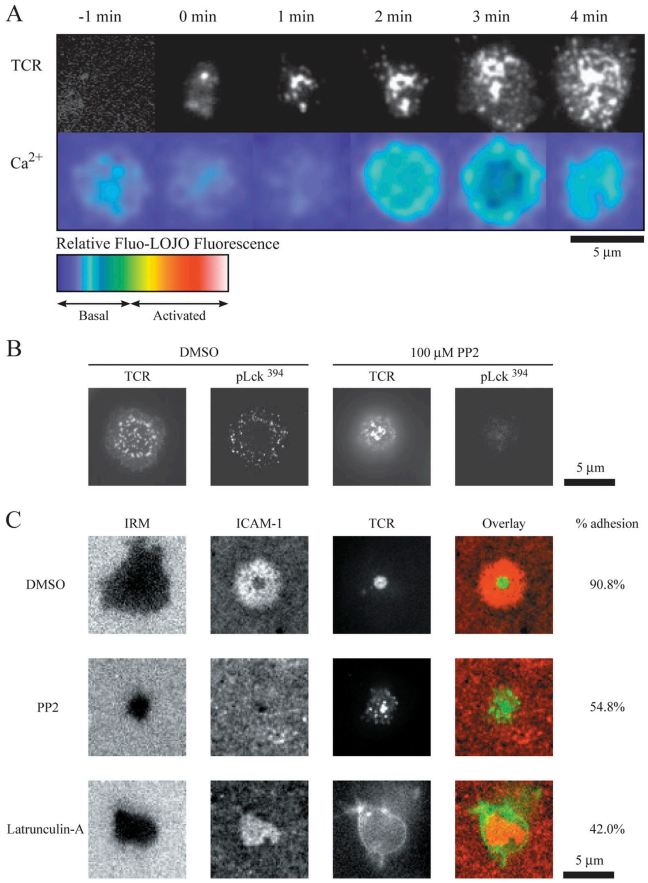

Figure 4. Effect of inhibition of Src family kinases and actin polymerization on TCR microclusters. Alexa546-H57 Fab–labeled AND TCR Tg T cells were incubated on bilayers containing ICAM-1 and MHCp after treatment by relevant drug vehicles, 10 μM PP2 or 1 μM latrunculin A. These concentrations inhibit Src family kinases and actin polymerization, respectively, >90% in intact cells. In each case, cells were treated with the drugs for 1 h before introduction to the planar bilayers. (A) TIRFM time course of TCR clustering (top) in the presence of inhibitory concentration of PP2. Activity of PP2 was verified by lack of robust Ca^{2+} elevation (bottom). (B) Reduction of $pLck^{394}$ in TCR microclusters in the presence of 100 μM PP2 versus DMSO vehicle at 5 min. (wide-field images) Similar results were obtained by TIRFM. (C) Wide-field image of unlabeled AND T cell blasts on bilayers containing Oregon Green I-E^k (green in overlay) and Cy5 ICAM-1 (red in overlay) after cell treatment with vehicle, 10 μM PP2 or 1 μM latrunculin A, for 1 h before exposure to the bilayer for 1 h. The IRM image shows the contact area in darker gray. Individual fluorescence images are as indicated. The percent adhesion is indicted in the column adjacent to the images. Representative of three experiments each.

reflection microscopy (IRM), and reduced adhesion by 40% (Fig. 4 C). Thus, TCR microcluster formation was highly resistant to inhibition by PP2 (10–100 μM) compared with other down-stream effects of TCR signaling, but we cannot rule out that residual $pLck^{394}$ (<5%) in the TCR microclusters may contribute to their formation. Although ZAP-70 is not inhibited by PP2, its accumulation in TCR microclusters was reduced similarly to Lck (unpublished data).

We next asked if TCR microcluster formation was dependent upon actin cytoskeleton. The TCR is constitutively linked to actin, and TCR signaling induces a dramatic remodeling of the actin cytoskeleton to form the IS (25, 26). We used the actin monomer sequestering inhibitor latrunculin A to treat T cells before their introduction into the supported planar bilayer containing ICAM-1 and agonist MHCp. When T cells were pretreated with 1 μM latrunculin A they did not form any TCR microclusters, nor was there any evidence of TCR interaction with MHC–peptide complexes in the interface (Fig. 4 C). 42% of the T cells formed contact areas that were mediated by LFA-1–ICAM-1 interaction as demonstrated by ICAM-1 accumulation and IRM visualization of the contact areas. This was consistent with earlier studies that laterally mobile LFA-1 can engage ICAM-1 in cytochalasin D–treated lymphocytes (27). Thus, TCR microcluster formation requires participation of the actin cytoskeleton.

This series of experiments suggests that TCR microclusters are involved in early T cell signaling that is initiated by agonist MHCp, and that a second wave of smaller TCR microclusters may contribute substantially to sustained signaling. The formation of one to three TCR microclusters in small nascent contact areas was contemporaneous with the initiation of cytoplasmic Ca^{2+} increase. However, we found that signaling within the earliest TCR microclusters is transient and is stopped largely by 2–5 min, based on the reduction of activated phosphoforms of Lck, ZAP-70, and LAT. Activation of the tyrosine kinase cascade by 5 min was focused in the periphery of the IS, even after the first wave of microclusters had moved to the cSMAC. Sensitive TIRFM imaging revealed that new TCR clusters form in the periphery by 5 min, after the cSMAC is formed. The formation of microclusters was not blocked by >95% inhibition of $pLck^{394}$ production and total inhibition of Ca^{2+} increase and LFA-1 activation by PP2, but was blocked completely by depletion of actin filaments with latrunculin A.

These results suggest that microclusters may be primary, actin-dependent scaffolds for signaling. The role of actin in microcluster formation parallels its long established role in TCR signaling (28). The classic pathway for TCR regulation of actin requires an intact tyrosine kinase cascade that is initiated by Src family kinases (29–31). TCR microclusters are highly resistant to inhibition by PP2. However, the microclusters that formed in the presence of PP2 contained detectable $pLck^{394}$ and $pZAP^{319}$; further work is needed to determine if different mechanisms for actin regulation are involved in microcluster formation compared with down-stream signals.

The supported planar bilayer system combines advantages of anti-CD3–coated glass and APCs. The ability to apply TIRFM is an advantage of anti-CD3–coated glass and glass-supported planar bilayers (32, 33). The planar bilayer system is more physiologic than anti-CD3–coated surfaces in that defined cell adhesion molecules and agonist

MHCp are incorporated—and when anchored to lipids—are laterally mobile as on APCs (34). Mobility of the bilayer allows formation of SMACs (2, 5). Although single MHCp can be counted in snapshots of the T cell–APC interface (35), the supported planar bilayers can be used to track single molecules over time (32, 33). The planar bilayer system is less physiologic than APCs, because the number of APC components incorporated into the bilayers is limited, the diffusion coefficients are faster in the supported bilayer than in cellular systems, and the surface is rigidly two-dimensional, unlike three-dimensional APC membranes. This property of forcing the interface into two dimensions may promote organization of the IS into SMACs more readily than three-dimensional APCs (8). We used high densities of agonist MHCp compared with the limiting case of ~10 MHCp in the IS defined by T cell–APC studies (35). However, in the latter case, thousands of self-MHCp also contribute to the activation process and make it likely that microclusters with many TCRs contribute (35, 36). Our study used the supported planar bilayer model to advance the general understanding of TCR microclusters—structures that are well documented in T cell–APC systems—by taking advantage of TIRFM and the ability to manipulate agonist MHCp density over a wider range than is possible with APCs.

Our finding extends those obtained with anti-CD3 substrates that show signaling by small TCR clusters in seconds that are resistant to PP2, but are dependent upon actin (12). It was not known if these characteristics were related to anti-CD3 or intrinsic to TCR recognition of physiologic ligands. The stimulation of normal T cells with mobile MHCp results in a highly ordered signaling structure in which the cSMAC has relatively low tyrosine kinase activation and the pSMAC contains foci of efficient tyrosine kinase activation. These distinct compartments have not been documented with anti-CD3 on glass (12, 14, 32). Our results with physiologic affinity MHCp reveal that there is an active process of MHC microcluster formation that precedes Ca^{2+} elevation and is dependent upon f-actin. Probing the mechanism of f-actin–dependent cluster formation may lead to new approaches to control of T cell signaling through manipulation of the microcluster scaffold.

MATERIALS AND METHODS

Materials. The H57 (anti-TCRβ) hybridoma was obtained from American Type Culture Collection. The acetoxymethyl ester form of the calcium sensitive, cell leakage resistant dye Fluo-LOJO, was purchased from Teflabs. All other reagents were obtained from Sigma-Aldrich. PP2 (4-amino-5-[4-chlorophenyl]-7-[t-butyl]pryazolo[3,4-d]pyrimidine) was purchased from Calbiochem.

Mice and cell culture. B10.Cg-Tg (TcrAND) 53Hed/J (B10.AND), TCR transgenic mice were purchased from The Jackson Laboratory and were crossed to B10.Br mice.

AND TCR Tg spleen cells were activated in DMEM (Invitrogen) with 10% FBS (Hyclone) using 1 μM MCC peptide (MCC88-103). At 48 h, the cells were washed twice in complete medium and were plated at 10^6 cells/ml with 50 U/ml of rIL-2. The cells were replenished with fresh media and IL-2 every 2 d. Experiments were performed on T cells between 6 and 15 d after activation.

Bilayers. Glass-supported dioleoylphosphatidylcholine bilayers incorporating GPI-anchored forms of unlabeled I-E^k (200 molecules/μm^2 total) and unlabeled or Cy5–ICAM-1 (300 molecules/μm^2) were prepared in Bioptechs flow cell (5). The bilayers were loaded with 100 μM MCC88-103 peptide (5).

Phosphoprotein staining. T cells were fixed with 2% formaldehyde for 12 min, permeabilized with 0.05% Triton X-100 for 1 min, blocked with 5% casein for 20 min, and stained with anti phospho–ZAP-70^{319} (Cell Signaling), anti–phospho-LAT^{191} (Upstate Biotechnology), and anti phospho-Lck^{394} specific affinity purified rabbit antibody (A. Shaw, Washington University School of Medicine, St. Louis, MO). An Alexa Fluor-488 goat anti–rabbit $F(ab')_2$ (Invitrogen) was used as secondary antibody.

Microscopy. All microscopy was performed on an automated microscope with an Olympus TIRFM module (17) and a Hamamatsu USA Orca-ER cooled CCD camera. The hardware on the microscope was controlled using IPLAB software (Scanalytics) on a PowerMac G4 Macintosh computer. Solamere Technology provided integration support.

Imaging of TCR and phosphoprotein staining. AND T cells were suspended in Hepes buffered saline supplemented with 5 mM glucose, 2 mM $MgCl_2$, 1 mM $CaCl_2$, and 1% human serum albumin (HBS/HSA), and were labeled with 10 μg/ml Alexa488 or 546 conjugated H57 Fab. The labeled cells were made to interact with the bilayers at 37°C. For TIRFM, the Fab was present continuously during imaging. In wide-field or TIRFM mode, images were exposed for 1–2 s, at a resolution of 0.11 μm per pixel using the 60× 1.45 N.A. objective. Images were inspected using Metamorph (Molecular Devices). Quantification of the signaling efficiency, based upon phosphoprotein and TCR intensities, was performed in IPLAB. Colocalization by area was analyzed using this function of Volocity (Improvision).

Estimation of initial microcluster size. H57 binding sites on T cell blasts were determined by flow cytometry with fluorescein calibration beads (Bangs Labs) to be 42,000 per cell (140 per μm^2). Microclusters were two times the average intensity of MHCp of 50 molecules/μm^2. Therefore, 140 TCRs were present in 0.35–0.5 μm^2 area.

Calcium measurements. AND T cells were labeled with 3 μM of Fluo-LOJO ($K_{Ca}2^+$ = 440 nM). Images with ionomycin in normal and no Ca^{2+} buffers were used to set minimum and maximum levels for display of relative Fluo-LOJO fluorescence. Basal and activation associated ranges were defined based on measurements on cells on ICAM-1 (basal range) or ICAM-1 plus agonist MHCp (activated range).

We thank T. Starr for expert technical assistance and A. Shaw for the phospho-Lck^{394} specific affinity purified antibody.

G. Campi is supported by a graduate fellowship from Boehringer Ingelheim Fonds, R. Varma is supported by a Bernard Levine Fellowship, and M.L. Dustin is supported by National Institutes of Health AI43542 and GM 64900.

The authors have no conflicting financial interests.

Submitted: 13 June 2005
Accepted: 29 August 2005

REFERENCES

1. Krogsgaard, M., and M.M. Davis. 2005. How T cells "see" antigen. *Nat. Immunol.* 6:239–245.
2. Monks, C.R., B.A. Freiberg, H. Kupfer, N. Sciaky, and A. Kupfer. 1998. Three-dimensional segregation of supramolecular activation clusters in T cells. *Nature.* 395:82–86.
3. Bromley, S.K., W.R. Burack, K.G. Johnson, K. Somersalo, T.N. Sims,

C. Sumen, M.M. Davis, A.S. Shaw, P.M. Allen, and M.L. Dustin. 2001. The immunological synapse. *Annu. Rev. Immunol.* 19:375–396.
4. Huppa, J.B., and M.M. Davis. 2003. T-cell-antigen recognition and the immunological synapse. *Nat. Rev. Immunol.* 3:973–983.
5. Grakoui, A., S.K. Bromley, C. Sumen, M.M. Davis, A.S. Shaw, P.M. Allen, and M.L. Dustin. 1999. The immunological synapse: a molecular machine controlling T cell activation. *Science.* 285:221–227.
6. Lee, K.H., A.D. Holdorf, M.L. Dustin, A.C. Chan, P.M. Allen, and A.S. Shaw. 2002. T cell receptor signaling precedes immunological synapse formation. *Science.* 295:1539–1542.
7. Freiberg, B.A., H. Kupfer, W. Maslanik, J. Delli, J. Kappler, D.M. Zaller, and A. Kupfer. 2002. Staging and resetting T cell activation in SMACs. *Nat. Immunol.* 3:911–917.
8. Lee, K.H., A.R. Dinner, C. Tu, G. Campi, S. Raychaudhuri, R. Varma, T.N. Sims, W.R. Burack, H. Wu, J. Wang, et al. 2003. The immunological synapse balances T cell receptor signaling and degradation. *Science.* 302:1218–1222.
9. Purtic, B., L.A. Pitcher, N.S. van Oers, and C. Wulfing. 2005. T cell receptor (TCR) clustering in the immunological synapse integrates TCR and costimulatory signaling in selected T cells. *Proc. Natl. Acad. Sci. USA.* 102:2904–2909.
10. Krummel, M.F., M.D. Sjaastad, C. Wulfing, and M.M. Davis. 2000. Differential clustering of CD4 and CD3ζ during T cell recognition. *Science.* 289:1349–1352.
11. Johnson, K.G., S.K. Bromley, M.L. Dustin, and M.L. Thomas. 2000. A supramolecular basis for CD45 regulation during T cell activation. *Proc. Natl. Acad. Sci. USA.* 97:10138–10143.
12. Bunnell, S.C., D.I. Hong, J.R. Kardon, T. Yamazaki, C.J. McGlade, V.A. Barr, and L.E. Samelson. 2002. T cell receptor ligation induces the formation of dynamically regulated signaling assemblies. *J. Cell Biol.* 158:1263–1275.
13. Jordan, M.S., A.L. Singer, and G.A. Koretzky. 2003. Adaptors as central mediators of signal transduction in immune cells. *Nat. Immunol.* 4:110–116.
14. Barda-Saad, M., A. Braiman, R. Titerence, S.C. Bunnell, V.A. Barr, and L.E. Samelson. 2005. Dynamic molecular interactions linking the T cell antigen receptor to the actin cytoskeleton. *Nat. Immunol.* 6:80–89.
15. McConnell, H.M., T.H. Watts, R.M. Weis, and A.A. Brian. 1986. Supported planar membranes in studies of cell-cell recognition in the immune system. *Biochim. Biophys. Acta.* 864:95–106.
16. Huppa, J.B., M. Gleimer, C. Sumen, and M.M. Davis. 2003. Continuous T cell receptor signaling required for synapse maintenance and full effector potential. *Nat. Immunol.* 4:749–755.
17. Schmoranzer, J., M. Goulian, D. Axelrod, and S.M. Simon. 2000. Imaging constitutive exocytosis with total internal reflection fluorescence microscopy. *J. Cell Biol.* 149:23–32.
18. Oheim, M. 2001. Imaging transmitter release. II. A practical guide to evanescent-wave imaging. *Lasers Med. Sci.* 16:159–170.
19. Wulfing, C., M.D. Sjaastad, and M.M. Davis. 1998. Visualizing the dynamics of T cell activation: intracellular adhesion molecule 1 migrates rapidly to the T cell/B cell interface and acts to sustain calcium levels. *Proc. Natl. Acad. Sci. USA.* 95:6302–6307.
20. Holdorf, A.D., K.H. Lee, W.R. Burack, P.M. Allen, and A.S. Shaw. 2002. Regulation of Lck activity by CD4 and CD28 in the immunological synapse. *Nat. Immunol.* 3:259–264.
21. Di Bartolo, V., D. Mege, V. Germain, M. Pelosi, E. Dufour, F. Michel, G. Magistrelli, A. Isacchi, and O. Acuto. 1999. Tyrosine 319, a newly identified phosphorylation site of ZAP-70, plays a critical role in T cell antigen receptor signaling. *J. Biol. Chem.* 274:6285–6294.
22. Zhang, W., R.P. Trible, M. Zhu, S.K. Liu, C.J. McGlade, and L.E. Samelson. 2000. Association of Grb2, Gads, and phospholipase C-gamma 1 with phosphorylated LAT tyrosine residues. Effect of LAT tyrosine mutations on T cell antigen receptor-mediated signaling. *J. Biol. Chem.* 275:23355–23361.
23. Hanke, J.H., J.P. Gardner, R.L. Dow, P.S. Changelian, W.H. Brissette, E.J. Weringer, B.A. Pollok, and P.A. Connelly. 1996. Discovery of a novel, potent, and Src family-selective tyrosine kinase inhibitor. Study of Lck- and FynT-dependent T cell activation. *J. Biol. Chem.* 271:695–701.
24. Tatton, L., G.M. Morley, R. Chopra, and A. Khwaja. 2003. The Src-selective kinase inhibitor PP1 also inhibits Kit and Bcr-Abl tyrosine kinases. *J. Biol. Chem.* 278:4847–4853.
25. Rozdzial, M.M., B. Malissen, and T.H. Finkel. 1995. Tyrosine-phosphorylated T cell receptor zeta chain associates with the actin cytoskeleton upon activation of mature T lymphocytes. *Immunity.* 3:623–633.
26. Dustin, M.L., and J.A. Cooper. 2000. The immunological synapse and the actin cytoskeleton: molecular hardware for T cell signaling. *Nat. Immunol.* 1:23–29.
27. Kucik, D.F., M.L. Dustin, J.M. Miller, and E.J. Brown. 1996. Adhesion-activating phorbol ester increases the mobility of leukocyte integrin LFA-1 in cultured lymphocytes. *J. Clin. Invest.* 97:2139–2144.
28. Valitutti, S., M. Dessing, K. Aktories, H. Gallati, and A. Lanzavecchia. 1995. Sustained signalling leading to T cell activation results from prolonged T cell receptor occupancy. Role of T cell actin cytoskeleton. *J. Exp. Med.* 181:577–584.
29. Bubeck Wardenburg, J., R. Pappu, J.Y. Bu, B. Mayer, J. Chernoff, D. Straus, and A.C. Chan. 1998. Regulation of PAK activation and the T cell cytoskeleton by the linker protein SLP-76. *Immunity.* 9:607–616.
30. Lin, J., and A. Weiss. 2001. T cell receptor signalling. *J. Cell Sci.* 114: 243–244.
31. Su, I.H., M.W. Dobenecker, E. Dickinson, M. Oser, A. Basavaraj, R. Marqueron, A. Viale, D. Reinberg, C. Wulfing, and A. Tarakhovsky. 2005. Polycomb group protein ezh2 controls actin polymerization and cell signaling. *Cell.* 121:425–436.
32. Douglass, A.D., and R.D. Vale. 2005. Single-molecule microscopy reveals plasma membrane microdomains created by protein-protein networks that exclude or trap signaling molecules in T cells. *Cell.* 121: 937–950.
33. Klopfenstein, D.R., M. Tomishige, N. Stuurman, and R.D. Vale. 2002. Role of phosphatidylinositol(4,5)bisphosphate organization in membrane transport by the Unc104 kinesin motor. *Cell.* 109:347–358.
34. Bierer, B.E., S.H. Herrmann, C.S. Brown, S.J. Burakoff, and D.E. Golan. 1987. Lateral mobility of class I histocompatability antigens in B lymphoblastoid cell membranes: modulation by cross-linking and effect of cell density. *J. Cell Biol.* 105:1147–1152.
35. Irvine, D.J., M.A. Purbhoo, M. Krogsgaard, and M.M. Davis. 2002. Direct observation of ligand recognition by T cells. *Nature.* 419:845–849.
36. Krogsgaard, M., Q.J. Li, C. Sumen, J.B. Huppa, M. Huse, and M.M. Davis. 2005. Agonist/endogenous peptide-MHC heterodimers drive T cell activation and sensitivity. *Nature.* 434:238–243.